A model of thermally generated pH gradients in tapered capillaries

Xiao-Hong Fang, Marc Adams and Janusz Pawliszyn*

Department of Chemistry, University of Waterloo, Waterloo, Ontario, Canada N2L 3G1

Received 13th October 1998, Accepted 13th January 1999

Potential applied at the two ends of a tapered capillary can produce an electric field and a pH gradient at the same time. These fields will effect electrophoretic separation, if the diameters of capillaries are not uniform. In some cases these gradients can be used to our advantage. For example, this approach provides a simple way to perform isoelectric focusing without carrier ampholytes as Joule heat produced in the tapered capillary generates a temperature gradient, which in turn produces a pH gradient. A mathematical model is developed to analyze the temperature distribution along the tapered capillary axis. According to the model, the span of the temperature gradient increases with the increase in heat generated per volume of the capillary channel, and the slope of the gradient is determined by the steepness of the taper. The temperature profile predicted by the model is verified by measuring temperatures at the outer wall of the capillary. The calculated p*I* value of a sample protein, hemoglobin, which focuses in the thermally generated pH gradient, is near to its literature value. The model provides us with a better understanding of the heat transfer in a tapered capillary and theoretically demonstrates the potential of capillary isoelectric focusing separation with a tapered channel.

Isoelectric focusing (IEF) is an electrophoretic separation method in which amphoteric molecules are separated on the basis of differences in their isoelectric points. It has been regarded as an indispensable tool for the separation and characterization of bioparticles, such as proteins and polypeptides in biological and biomedical research.[1] The recently introduced capillary isoelectrophoretic focusing (CIEF), which was first developed by Hjerten and Zhu,[2] provides a new approach to performing IEF in free solution. As CIEF is characterized by its high speed, ease of automation and quantitation, interest in it is growing.[3–5]

Both conventional IEF and typical CIEF need to be conducted in a pH gradient formed by synthetic carrier ampholytes. The use of carrier ampholytes has many disadvantages.[1] The ampholytes are expensive and may interact with the samples. Moreover, they decrease the sensitivity of UV detection for proteins and bring difficulties for the recovery of separated fractions. Efforts have been made to create pH gradients without the use of carrier ampholytes. Methods include mixing buffers having different pH values,[6–7] sample autofocusing,[8] buffer electrofocusing,[9–11] changing the dielectric constant[12] or the temperature of the buffer,[13–16] and using controlled flows of solvolytical ions in a quadrupole electromigration column.[17]

Among those methods, utilizing a temperature gradient to create a thermally generated pH gradient is an effective way to establish a stable pH gradient in a short time. This can be achieved by locating two ends of the separation chamber in two baths with different temperatures;[13–16] however, the set-ups are complicated. A simple approach developed in our laboratory utilizes the Joule heat produced in a tapered capillary to generate a temperature gradient, which in turn produces a pH gradient. The feasibility of this method has been demonstrated previously by separating two components of human hemoglobin in a tapered capillary,[18] although the actual temperature and pH profiles produced were not determined. In this paper, a mathematical model describing the temperature distribution along the tapered capillary is developed. The model is verified experimentally and some factors which affect the temperature and pH gradients are discussed. With this mathematical model, one can design the capillary shape and choose other suitable experimental conditions to get a desired pH gradient.

Model development

Fig 1 depicts the longitudinal section of an ideal tapered capillary. The outer diameter of the capillary is constant (R) while its inner diameter (r) is a linear function of the position along axis z. When current is passed through the capillary, the amount of heat generated increases as the capillary inner diameter decreases, which causes a temperature gradient in the axial direction. On the other hand, the loss of heat from the outer wall of the capillary to the surroundings results in a temperature drop in the radial direction. The temperature profile along the capillary can be derived by solving differential equations describing heat transfer in the capillary system. When the capillary is assumed to be symmetrical along its axis, temperature at any point inside the capillary is determined by its axial and radial positions. Because it is complex to solve equations for a two-dimensional heat transfer analysis, we simplified the problem using a one-dimensional model.

If there is no heat transfer along the axial direction, temperature distribution in the radial direction can be determined by the same method used in the case of a regular

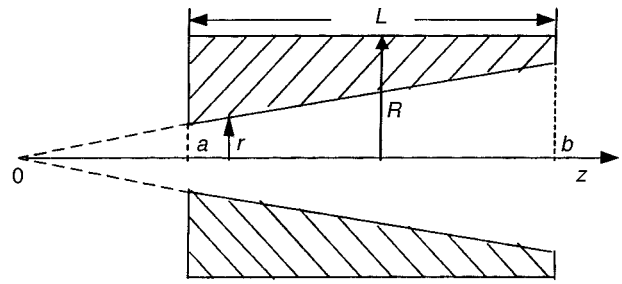

Fig. 1 Longitudinal section of a tapered capillary.

capillary.[19,20] The temperature drop (ΔT) from the center of the capillary to the surroundings is given by:

$$\Delta T = \frac{Qr_1^2}{2}\left[\frac{1}{2K_1} + \frac{1}{K_2}\ln\left(\frac{r_2}{r_2}\right) + \frac{1}{r_2 h}\right] \quad (1)$$

where Q is the heat generation rate, K_1 and K_2 are the thermal conductivity of buffer and capillary wall, r_1, r_2 are the inner and outer radii of the capillary and h is the capillary–air heat transfer coefficient. The thicknesses of the capillary inner and outer coatings are ignored in equation (1). As the resistance to heat transfer between the wall of the capillary and air is typically much larger than other resistances inside the capillary, ΔT is dominated by the last term in equation (1).[20] According to our calculation, the temperature difference from the center of the capillary to its outer wall (ΔT_{cap}) contributes less than 10% of overall radial temperature drop in the tapered capillaries used. Moreover, the radial temperature drop and its dependence on the boundary conditions are greatest under the condition that no heat transfer occurs in the axial direction. Therefore, ΔT_{cap} can be ignored and the electrolyte and the capillary can be assumed to be at a uniform temperature over the cross-section when axial heat transfer is considered. Thus, we assume the temperature at any point inside the capillary is determined only by the position along the axial direction of the capillary.

Other assumptions for the one dimensional model are as follows (1) The capillary has a perfect taper shape so that the inner radius of the capillary (r) is given by $r = zm$ (m is a constant, $a < z < b$, see Fig. 1). (2) For the capillary with ends in two buffer reservoirs, the temperatures at the two end-points are equal to the temperatures of the buffers in the reservoirs, which in this case is the room temperature. Room temperature is treated as zero for mathematical convenience. (3) The system is under a steady state condition; thus the current passing through the tapered capillary is a constant and temperatures along the capillary do not change with time ($dT/dt = 0$). (4) There is no electroosmotic flow inside the capillary due to the effective coating. (5) The changes in the buffer conductivity are neglected.

With the above assumptions, the heat transfer equation is:[21]

$$\frac{\partial}{\partial z}\left(K(z)\frac{\partial T}{\partial z}\right) - \frac{2hT}{R} + q = 0 \quad (2)$$

with boundary conditions $T(a) = 0$, $T(b) = 0$.

In equation (2), T stands for the temperature of the capillary, h is the capillary–air heat transfer coefficient calculated using the method developed by Mikheyev[22] for natural convection and $K(z)$ is the capillary's thermal conductivity, which is the volume average of the thermal conductivity of electrolyte (K_1) and capillary wall (K_2):

$$K(z) = K_2\left[1 - \left(1 - \frac{K_1}{K_2}\right)\left(\frac{mz}{R}\right)^2\right] \quad (3)$$

where q is the heat generation per volume of the capillary

$$q = \frac{I^2}{\sigma\pi^2 R^2 m^2 z^2} \quad (4)$$

and σ is the electric conductivity of the buffer.

By substituting (3) and (4) into (2) and letting,

$$z = x\frac{R}{m}\left(1 - \frac{K_1}{K_2}\right)^{-\frac{1}{2}}$$ we get

$$\frac{\partial}{\partial_x}\left[\left(1 - x^2\right)\frac{\partial}{\partial x}T\right] - v\,T + \frac{G}{x^2} = 0 \quad (5)$$

where

$$v = \frac{2hR}{K_2 m^2}\left(1 - \frac{K_1}{K_2}\right)^{-1}$$

$$G = \frac{I^2}{\sigma K_2 \pi^2 R^2 m^2}$$

Although equation (5) can be solved by a series solution (See Appendix A), the solution can be further simplified. Since the change in $K(z)$ along the capillary is relatively small, $K(z)$ can be approximately treated as a constant, so the term $1\text{-}x^2$ can be substituted by its average value. Equation (5) thus becomes

$$\frac{\partial^2}{\partial x^2}T - v'^2 T + \frac{G'}{x^2} = 0 \quad (6)$$

where $v' = \sqrt{(v/c)}$, $G' = G/c$,

$$c = \frac{\int_{x_1}^{x_2}\left(1 - x^2\right)\mathrm{d}x}{x_2 - x_1}$$

and x_1, x_2 are the values resulting when $z = a$ and $z = b$, respectively.

The solution to equation (6) generated using Maple software (Maple V Release 4, Waterloo Maple Inc., Waterloo, Canada) is:

$$v(x) = \frac{G'}{2}\left[\mathrm{e}^{v'x}Ei(1, v'x) + \mathrm{e}^{-v'x}Ei(1, -v'x)\right] + \mathrm{A}\mathrm{e}^{v'x} + \mathrm{B}\mathrm{e}^{-v'x} \quad (7)$$

where A and B are chosen to satisfy the boundary conditions at the end-points $T(x) = 0$ at $z = a$ and $z = b$. *Ei* is the 'exponential integral' defined by Maple as:

$$Ei(n, x) = \int_1^\infty \frac{\mathrm{e}^{-xt}}{t^n}\mathrm{d}t$$

The temperature profile determined in the capillary modelled approximately by solution (7) is very close to that modelled by the exact solution to equation (5), solution (11) in Appendix A. Fig. 2 shows that there is less than 4% deviation for the typical tapered capillary used. Therefore, equation (7) is used to mathematically model the temperature distribution inside the capillary. Using the Maple software, graphical representations of the mathematical model were obtained for theoretical study. The model was also verified experimentally.

Using the same assumptions and coordinates, two other models have also been developed for the tapered capillary, with either constant wall thickness or proportional wall thickness (Appendices B and C). The temperature profiles obtained from

these models are similar to that from the above model [solution (7)]. Thus, temperature gradients produced in tapered capillaries with different geometric shapes are similar.

Experimental

Three tapered capillaries (Polymicro Technology, Phoenix, AZ, USA) with the same outer diameter but different inner diameters were used. The capillaries were coated with linear polyacryamide as previously reported[18] to eliminate electroosmotic flow. A 25 mM Tris (Bio-Rad, Hercules, CA, USA) solution was prepared in deionized water and its pH was adjusted to 7.32 (23 °C) by HCl. Dog hemoglobin (Sigma, St. Louis, MO) solution was prepared in Tris–HCl buffer (3 mg ml^{-1}).

During the experiment, the capillary was mounted horizontally on a cartridge with its ends immersed in two 6 mL buffer reservoirs. The separation was driven by a high voltage dc power supply (RE-3002B, Northeast Scientific Corporation, Cambridge, Massachusetts, USA). The anode was inserted into the buffer reservoir at the capillary end with the narrower inner diameter. A 10 kΩ resistor was connected between the cathode and the ground. Its voltage was measured by a multimeter in order to monitor the current in the system.

For temperature measurement, the capillary and the reservoirs were filled with Tris–HCl buffer. After applying the voltage for about 20 min, the temperatures along the capillary outer wall were measured using thermocouples (Chromega–Alomega, 0.127 mm, Omega Engineering Inc., Stamford, CT, USA).

For isoelectric focusing of the protein, voltage was applied for about 8 min before the injection of sample. Then a few drops of hemoglobin solution were added to the catholyte. The focused zone of hemoglobin was detected by CCD absorption imaging detection. This detection system consists simply of a halogen video camera lamp (Henderson, Stockholm, Sweden) powered by a camcorder battery (Sony), a 390–420 nm bandpass filter (Melles Griot, Irvine, CA, USA) and a CCD camera (Sony, Model XC-77CE) with a 1 : 2.8, 50 mm objective (Sony). The setup for monitoring the isoelectric focusing of sample was similar to that reported previously.[23] The CCD camera was controlled by PC computer with image acquisition hardware (Data Translation's frame grabber board, Vision-EZ™, Marlboro, MA, USA) and a data analysis software (Gobal Lab, Data Translation). The light intensities from the image profiles were transferred to Microsoft Excel to produce an absorption electropherogram.

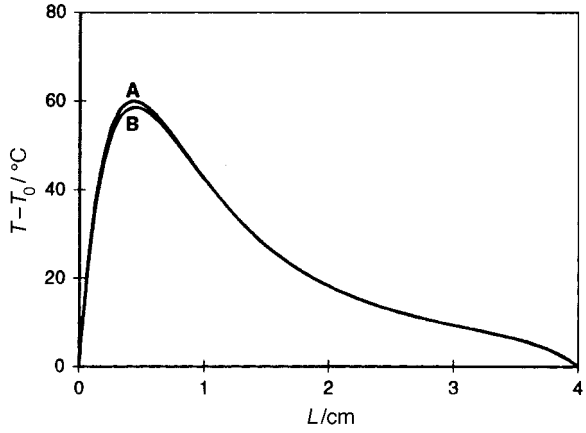

Fig. 2 Temperature profiles for the approximate solution (A) and the exact solution (B) of the model. T_o refers to the room temperature. Conditions: capillary L = 4 cm, r_1 = 50 μm, r_2 = 300 μm, R = 450 μm; current I = 200 μA; others h = 35 W m^{-2} K^{-1}; σ = 0.22 Ω^{-1}, K_1 = 0.6 W m^{-1} K^{-1}; K_2 = 1.5 W m^{-1} K^{-1}.

Results and discussion

Model verification for temperature gradient

Measuring the temperature of the outer wall capillary gave us an approximate temperature profile inside the capillary. Temperatures measured under two current levels are shown with the temperature profiles calculated by the model, Fig. 3 A and B.

The results indicate that the measured temperatures at most positions along the capillary agreed with the calculated temperature profiles. Obvious differences between the measured and the calculated values were only found at the two ends of the capillary. In the rest of the capillary, the small discrepancies may have been caused by the small temperature difference existing between the temperature measured by the thermocouple and the exact temperature of the capillary.

At the ends of the capillary, especially at the narrow end, the temperature difference between the measured and calculated values is caused by the end-point effect. As about 0.2 cm of the capillary at each end was immersed in the buffer solution, the large heat loss in these sections results in a temperature decrease nearby. Shortening the length of the sections in the buffer can reduce this effect. The exact temperature profile in this area may be obtained by developing the two dimensional model for the heat transfer analysis.

pH gradient

When the capillary is filled with a buffer that has a weak acid or weak basic constituent, the temperature gradient along the capillary will produce a corresponding pH gradient. This is mainly due to the thermodynamic property of the dissociation constant of the buffer.

The temperature dependence of the hydrogen ion activity (α_H) of a buffer solution composed of a single weak acid and its salts can be expressed as[24]

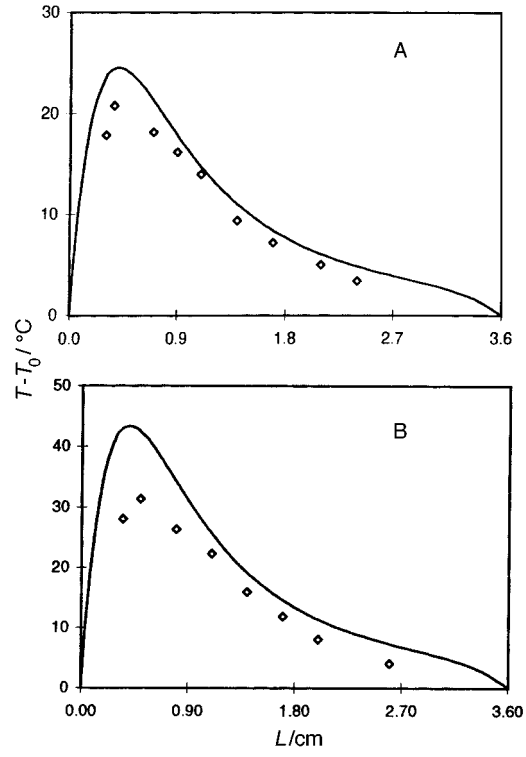

Fig. 3 Comparison of the measured temperatures (diamonds) and the calculated temperature profile (line). Conditions: (A) I = 118 μA, (B) I = 160 μA; capillary r_1 = 49 μm, r_2 = 297 μm, L = 3.6 cm; T_o is 23 °C; for others see Fig 2.

$$\frac{\partial p\alpha_{H}}{\partial T} \approx -\frac{\partial \ln K}{\partial T} = -\frac{\Delta H^{0}}{RT^{2}} \quad (8)$$

where K is the dissociation constant of the acid, R is the gas constant and ΔH^0 is the molar heat of dissociation of the acid.

Among the common buffers, Tris–HCl is recognized as the buffer which has the largest temperature coefficient of pH (dpH/dT = −0.028 units per degree at 25 °C). Its pK_a has an approximately linear relationship with temperature from 0–80 °C.[25] A more accurate equation to express the change of its pK_a with the temperature (T from 273 K to 323 K) was obtained by Bates[26]

$$\log K_a = \frac{2984.1}{T} - 3.5888 + 0.005571T \quad (9)$$

Therefore, by knowing the temperature gradient inside the capillary, the corresponding pH gradient can be obtained.

Several other buffers also have high temperature coefficients,[27–28] including cholamine chloride (pK = 7.1, dpH/dT = −0.027 at 20 °C), glycylglycine (pK = 8.25, dpH/dT = −0.026 at 25 °C), 2-amino-2-methyl-1,3-propanediol (pK = 8.79, dpH/dT = −0.029 at 25 °C). These could also be used to form thermally generated pH gradients in different pH ranges. The general character of these buffers is that they all have amino groups as the ionization groups. As the amino group has a large ΔH^0 , their dln$K$/dT are larger than other kinds of buffers.

Temperature also has an effect on the pI of the sample protein. Except for the carboxyl group, the protolytic groups, especially amino groups in proteins, have large molar heats of ionization.[29] Focusing of protein occurs only if $(\mathrm{dpH}/\mathrm{d}T)_{\mathrm{buff}} - (\mathrm{dp}I/\mathrm{d}T)_{\mathrm{pro}} \neq 0$. A thermally generated pH gradient is expected to be advantageous for focusing acidic and neutral proteins as they usually have more carboxyl groups. For focusing basic proteins, the pI values of which are sensitive to temperature changes, buffers with low dpH/dT can be used.

Protein focusing

Potential applied at two ends of a tapered capillary produces an electric field and a pH gradient at the same time which can be used for the focusing of protein. Two isoforms of human hemoglobin were focused and separated earlier using the tapered capillary.[18] In the present work, focusing of dog hemoglobin is shown. The established pI value of dog hemoglobin is 6.91 at 6 °C.[30] When injected into the cathodic buffer at pH 7.32, it was negatively charged and moved into the capillary by electrophoretic force. As there was a pH gradient inside the capillary, the protein gradually lost its negative charge during its migration to the narrow end of the capillary. Finally, it focused at the position where its charge was zero. An electropherogram of the focused protein is shown in Fig. 4. The pI value calculated by the model, according to the focusing position, is 6.81, which is in good agreement with its literature pI value.

Another example of the focusing is shown in Fig. 5. The absorption increased with the focusing time from A to B and C to D, indicating an accumulation of the protein inside the capillary. Its accumulation rate increased as the voltage increased. Also when voltage was increased, a larger pH gradient was formed, causing the focusing position to shift to the wide end of the capillary. The width of the protein band was also increased at the position with wider inner diameter.

As we know:

$$\frac{\mathrm{dpH}}{\mathrm{d}z} = \frac{\mathrm{dpH}}{\mathrm{d}T} \times \frac{\mathrm{d}T}{\mathrm{d}z} \quad (10)$$

By substituting (7), (8) and (9) into (10), the change in pH gradient along the capillary can be calculated. From our calculation, dpH/dz at the focusing position in Fig. 5 (D) is about 7.0, which is larger than that in (B) (which is about 4.5). Moreover, although the current increased from (B) to (D), the field strength ($E = I/\sigma\pi r^2$) in (D) was still lower than that in (B) because of the different diameters. It is known that good resolution in IEF is favored by a high field strength and a shallow pH gradient.[24] Therefore, the resolution in (D) is worse than in (B). The resolution can also be adversely affected by the gradients present in the radial direction of the capillary. To minimize this effect thin capillaries should be used.

Properties of the temperature gradient

According to equation (10), the pH gradient in a tapered capillary is mainly determined by the temperature gradient. Therefore, the properties of the temperature gradient reflect the properties of the pH gradient. With the help of the mathematical

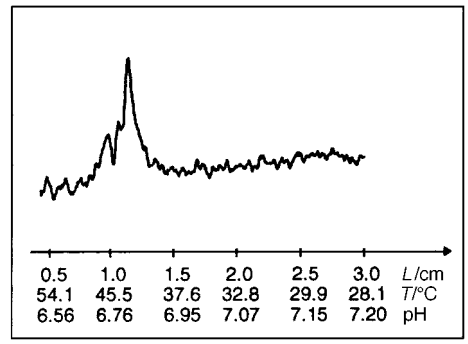

Fig. 4 Electropherogram of focused hemoglobin. Conditions: capillary r_1 = 27 μm, r_2 = 154 μm, L = 4.0 cm; current I = 70 μA, voltage U = 1000 V.

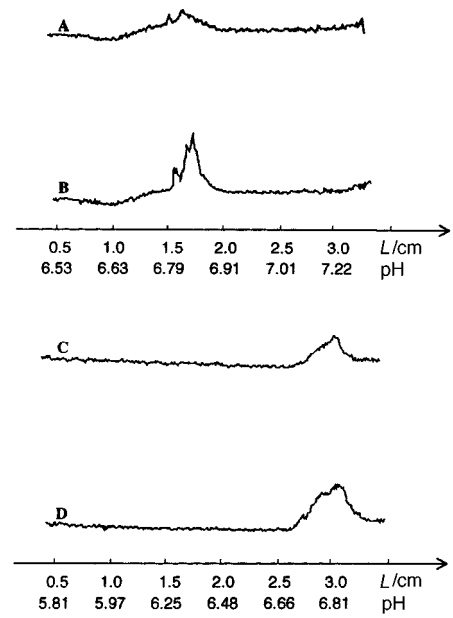

Fig 5 Electropherogram of focused hemoglobin under different voltages. Conditions: capillary r_1 = 90 μm, r_2 = 270 μm, L = 3.7 cm; (A) 15 min, (B) 35 min after sample injection under 900 V voltage and 200 μA current; (C) 15 min and (D) 20 min after sample injection under 1200 V voltage and 290 μA current.

model, temperature gradient profiles along a tapered capillary under different conditions can easily be obtained. Factors that affect the temperature gradient can be derived from equation (7) and studied by computer simulation.

Effect of the current

The current passing through the capillary is an important parameter which determines the Joule heat produced inside the capillary, and thus the temperature gradient. The higher the current which is applied in the system, the greater the amount of heat generated inside the capillary and the larger the temperature difference it produces. As shown in Fig 6, the maximum temperature difference (T_{max}) increases from 18 to 72 °C when the current increases from 100 to 200 μA. T_{max} is proportional to the square of the current.

An understanding of this gives us a method for adjusting temperature and pH gradients during the experiment. An increase in current results in an increase in the range of the pH gradient for the focusing of analytes. However, there is a limitation on increasing current, as the possibilities of denaturation and precipitation of the proteins at high temperatures should be recognized. The pH range formed in the thermally generated gradient is normally 0.5–1 pH unit. As our experiments were performed at room temperature, the maximum temperature differences T_{max} were usually less than 40 °C for protein separation. Thus, actual temperatures within the capillary were in the range from 23 to 63 °C. Decreasing the ambient temperature by putting the whole capillary cartridge in a cold box for example, would allow the use of higher current.

Effect of the capillary shape

The span of the temperature gradient is also determined by the volume of the tapered channel. Changes in the length, outer diameter and wide and narrow end inner diameters of the capillary can all bring out changes in its volume and affect the temperature gradient. The smaller the volume is, the larger the temperature difference will be. As shown in Fig. 7, when a certain current is applied to capillaries that only have different wide end inner diameters, the temperature difference decreases with the increase of the wide end inner diameter.

If different tapered capillaries are used to obtain the same T_{max}, to get the same pH range for protein separation, the slope of the gradient is determined by the angle of the taper. In Fig. 8, a temperature difference of 50 °C is formed in the capillaries with different narrow end inner diameters. Their temperature profiles show different slopes. Smaller narrow end inner diameter tubing, which means a larger angle of the taper, results in a steeper temperature gradient. Meanwhile, when the angle of the taper is large, the temperature drop mainly occurs near the narrow end of the capillary, while a very shallow temperature gradient is present near the wide end of the capillary. Different slopes in the pH gradient can result in different resolving power for protein separation.

Therefore, by adjusting the system current and choosing a capillary with a suitable channel shape, one can get a desired pH profile for the separation of different samples on the basis of the theoretical calculation. Since the supply of tapered capillaries is limited, the experimental verification for model calculation concerned with the effect of the capillary shape cannot be obtained at present. It is expected that the use of tapered channels etched in a glass chip or silicon wafer will benefit the method development for obtaining the desired pH gradients. It should be emphasized that the temperature gradients in the system can be generated by using a uniform inside diameter capillary and varying the outside diameter because of the different amount of heat being lost through the wall of differing thickness. Also, by varying the buffer concentration different temperature gradients can be obtained for the same capillary design because of the different currents conducted through the system.

Acknowledgement

This work was jointly supported by the National Sciences and Research Council of Canada and Convergent Bioscience Ltd.

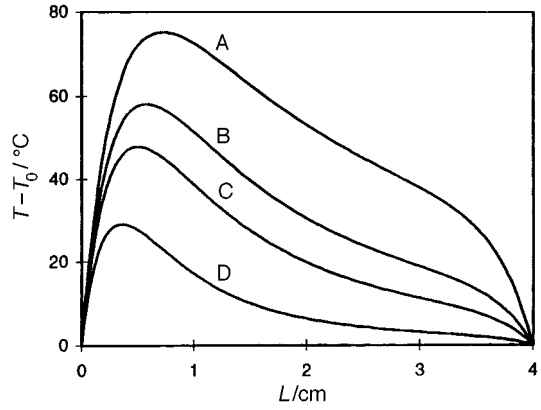

Fig. 7 Temperature profiles of tapered capillaries with different wide end inner diameters. Conditions: (A) r_2 = 100 μm; (B) r_2 = 150 μm; (C) r_2 = 200 μm; (D) r_2 = 400 μm; for others, see Fig. 2, I = 200 μA = constant.

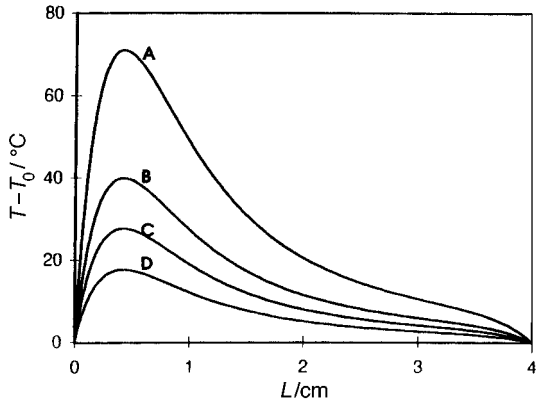

Fig. 6 Temperature profiles of a tapered capillary with different currents. Conditions are the same as those in Fig 2 except: (A) I = 200 μA; (B) I = 150 μA; (C) I = 125 μA; (D) I = 100 μA.

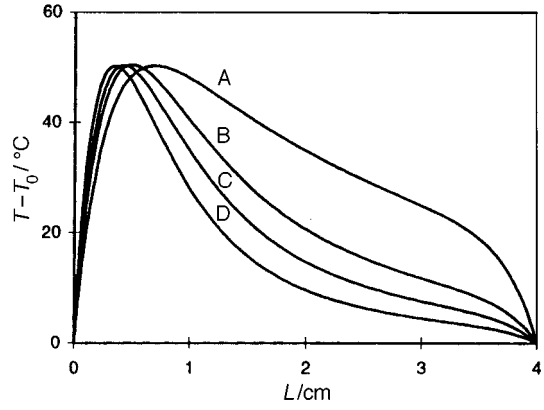

Fig. 8 Temperature profiles of tapered capillaries with different narrow end inner diameter. Conditions: (A) r_1 = 150 μm, I = 389 μA; (B) r_1 = 75 μm, I = 245 μA; (C) r_1 = 50 μm, I = 190 μA; (D) r_1 = 30 μm, I = 142 μA; for others, see Fig. 2, T_{max} = 50 °C.

We thank Heather Lord for editorial assistance in preparing this manuscript.

Appendices

Appendix A

The solution to the equation (5) is:

$$T(x) = GS'(x) + A\,Q'(x) + B\,'(x) \qquad (11)$$

where A and B are determined to satisfy the boundary conditions $T(x) = 0$ at $z = a$ and $z = b$, and

$$S'(x) = \ln x \sum_{n=0}^{\infty} a_n x^{2n} + \sum_{n=0}^{\infty} b_n x H^{2n}$$
$$= \left(a_0 + a_1x^2 + a_2x^4 + \ldots\right)\ln x + \left(b_0 + b_1x^2 + b_2x^4 + \ldots\right)$$

specified by

$$a_{n+1} = \frac{4n^2 + 2n + v}{4n^2 + 6n + 2}\mathrm{a_n},\ b_{n+1}$$
$$= \frac{4n^2 + 2n + v}{4n^2 + 6n + 2}\left[b_n + a_n\left(\frac{1+4n}{4n^2+2n+v} - \frac{1}{2n+2} - \frac{1}{2n+1}\right)\right]$$

for $n > 0$, and $a_0 = 1$, $b_0 = 0$.

$$v = \frac{2hR}{K_2m^2}\left(1 - \frac{K_1}{K_2}\right)^{-1}$$

$$Q'(x) = \sum_{n=0}^{\infty} \eta_n x^{2n} = 1 + \eta_1x^2 + \eta_2x^4 + \ldots,$$

$$\eta_{n+1} = \eta_n \frac{4n^2 + 2n + v}{4n^2 + 6n + 2},\ \eta_0 = 1$$

$$R'(x) = \sum_{n=0}^{\infty} \lambda_n x^{1+2n} = x + \lambda_1x^3 + \lambda_2x^5 + \ldots,$$

$$\lambda_n = \lambda_{n-1} \frac{4n^2 - 2n + v}{4n^2 + 2n},\ \lambda_0 = 1$$

Appendix B

The features of a capillary with proportional wall thickness are: its outer radius is $R = \mathrm{p}r$ (p is a constant); its average thermal conductivity, λ, is a constant $\{\lambda = [K_1 + (\mathrm{p}^2\text{-}1)K_2]/\mathrm{p}^2\}$ the heat transfer coefficient h changes when R changes. As h is approximately proportional to $R^{-1/2}$,[24] let $h = L/\sqrt{(\mathrm{p}mz)}$. The heat transfer equation to solve is

$$\frac{\partial}{\partial z}\left(z^2\frac{\partial}{\partial z}T\right) - v\sqrt{zT} + \frac{G}{z^2} = 0 \qquad (12)$$

where $v = \dfrac{2L}{(\mathrm{p}m)^{\frac{3}{2}}\lambda}$ and $G = \dfrac{I^2}{\lambda\sigma\pi^2\mathrm{p}^2m^4}$

The solution to (12) is:

$$T(z) = Gv^4S(x) + \frac{A}{\sqrt{x}}I_2\left(4x^{1/4}\right) + \frac{B}{\sqrt{x}}K_2\left(4x^{1/4}\right) \qquad (13)$$

where $x = v^2z$, A and B are determined to satisfy $T(x) = 0$ at $z = a$ and $z = b$, I_2, K_2 are Bessel functions, and

$$S(x) = -\frac{1}{2}x^{-2} - \frac{2}{3}x^{\frac{3}{2}} + \frac{2}{3}(\ln x + 1)x^{-1} - \frac{8}{3}(\ln x + 1)x^{\frac{1}{2}} + R(x)$$

$$R(x) = (\ln x)^2\sum_{n=0}^{\infty} a_n x^{\frac{n}{2}} + (\ln x)\sum_{n=0}^{\infty} b_n x^{\frac{n}{2}} + \sum_{n=0}^{\infty} c_n x^{\frac{n}{2}}$$

specified by

$$a_{n+1} = \frac{4}{(n+1)(n+3)}a_n$$

$$b_{n+1} = \frac{4}{(n+1)(n+3)}\left[b_n - 2(n+2)a_{n+1}\right]$$

$$c_{n+1} = \frac{4}{(n+1)(n+3)}\left[c_n - 2a_{n+1} - (n+2)b_{n+1}\right]$$

for $n > 0$, and $a_0 = -4/3$, $b_0 = 0$, $c_0 = 0$.

Appendix C

The features of a capillary with constant wall thickness are: the outer radius of the capillary is $R = mz$ and the inner radius is $r = m(z\text{-}c)$, where m and c are constants and $h = L/\sqrt{(mz)}$. Its heat transfer equation is:

$$\frac{\partial}{\partial z}\left(z^2\frac{\partial}{\partial z}T\right) - v\sqrt{zT} + \frac{G}{(z-c)^2} = 0 \qquad (14)$$

where $v = \dfrac{2L}{m^{\frac{3}{2}}\lambda}$ and $G = \dfrac{I^2}{\pi^2m^4\sigma\lambda}$

The solution is:

$$T(z) = R(x) + \frac{A}{\sqrt{x}}I_2\left(4x^{1/4}\right) + \frac{B}{\sqrt{x}}K_2\left(4x^{1/4}\right) \qquad (15)$$

where $x = v^2z$, A and B are determined to satisfy $T(x) = 0$ at $z = a$, $z = b$, and I_2, K_2 are Bessel functions.

$$R(x) = k_0S(x) + \sum_{s=1}^{2n-5} k_s x^{-2\frac{s}{2}} = K_0S(x) + k_1x^{\frac{5}{2}} + k_2x^{-3} + K_3x^{\frac{7}{2}} + \ldots$$

$$k_0 = C_2 - \sum_{n=3}^{\infty} h_{n[2n-5]} \text{ and } k_s = \sum_{n=\left\lfloor 2+\frac{s}{2}\right\rfloor}^{\infty} h_{n[2n-(s+4)]} \text{ for } s > 0$$

$$C_n = (n-1)c^{n-2}v^{2n}G,$$

$$h_{n(s+1)} = \frac{h_{ns}}{\left(n - \dfrac{2+1}{2}\right)\left(n - \dfrac{s+1}{2} - 1\right)},\ h_{n0} = -C_n/n(n-1)$$

$S(x)$ is defined above in Appendix B.

References

1 A. Kolin, in *Isoelectric Focusing*, ed. N. Catsimpoolas, Academic Press, New York, USA, 1976, pp. 1–11.
2 S. Hjerten and M-D. Zhu, *J.Chromatogr*. 1985, **346**, 265.
3 S. Hjerten, in *Capillary Electrophoresis: Theory and Practice*, ed. P. D. Grossman and J. C. Colburn, Academic Press, New York, USA, 1992, pp. 191–214.

4 T. Pritchett, in *Molecular Biology: Current Innovations and Future Trends*, ed. A. M. Griffin and H. G. Griffin, Horizon Scientific Press, Norwich, Norfolk, UK, 1995, pp. 127–145.
5 X. Liu, Z. Sosic and I. S. Krull, *J. Chromatogr.*, 1996, **735**, 165.
6 H. Rilbe, *J. Chromatogr.*, 1978, **159**, 193.
7 R. A. Mosher, W. Thormann, A. Graham and M. Bier, *Electrophoresis*, 1985, **6**, 545.
8 O. Sova, *J. Chromatogr*. 1985, **320**, 15.
9 R. L. Prestidge and M. T. Hearn, *Anal. Biochem*. 1977, **97**, 95.
10 A. Chrambach and N. Y. Nguyen, in *Electrofocusing and Isotachophoresis*, ed. B. J. Radola and D. Graesslin, Walter de Gruyter & Co., Berlin, Germany 1977, pp. 51–58.
11 L. M. Hjelmeland and A. Chrambach, *Electrophoresis*, 1983, **4**, 20.
12 G. V. Troitski, V. P. Savialov, I. F. Kirjukhin, V. M. Abramov and G. J. Agitski, *Biochim. Biophys. Acta*, 1975, **400**, 24.
13 S. J. Luner and A. Kolin, *Proc. Natl. Acad. Sci. U.S.A.* 1970, **66**, 898-903.
14 C. H. Lochmuller, S. J. Breiner and C. S. Ronsick, *J. Chromatogr*. 1989, **480**, 293.
15 P. Lundahl and S. Hjerten, *Ann. N. Y. Acad Sci.*, 1973, **209**, 94.
16 C. H. Lochmuller and C. S. Ronsick, *J. Chromatogr.*, 1991, **249**, 297.
17 J. Pospichal, M. Deml and P. Bocek, *J. Chromatogr.*, 1993, **638**, 179.
18 J. Pawliszyn and J. Wu, *J. Microcolumn Separations*, 1993, **5**, 397.
19 E. Grushka, R. M. McCormik and J. J. Kirkland, *Anal. Chem*., 1989, **6**, 241.
20 P. D. Grossman, in *Capillary Electrophoresis: Theory and Practice*, ed. P. D. Grossman and J. C. Colburn, Academic Press, New York, USA, 1992, pp. 5–9.
21 H. S. Carslaw and J. C. Jaeger, *Conduction of Heat in Solid*, Clarendon Press, Oxford, UK, 2nd edn., 1986, pp. 133–135.
22 M. Mikheyev, *Fundamentals of Heat Transfer*, Mir Publishers, Moscow, Russia, 1968, pp. 73–81.
23 A. Palm, C. Lindh, S. Hjerten and J. Pawliszyn, *Electrophoresis*, 1996, **17**, 766.
24 P. G. Righetti, *Isoelectric Focusing: Theory, Methodology and Applications*, Elsevier Biomedical Press, Amsterdam, The Netherlands, 1983.
25 L. P. Vonguyen, *Isoelectric Focusing With Cone-shaped Capillaries*, MSc Thesis, University of Waterloo, Waterloo, Canada, 1995.
26 R. G. Bates and H. B. Hetzer, *J. Phys. Chem*., 1961, **65**, 667.
27 D. D. Perrin and B. Dempsey, *Buffers for pH and Metal Ion Control*, Champman and Hall Ltd., London, UK, 1974, pp. 157–163.
28 R. M. C. Dawson, D. C. Elliott, W. H. Elliott and K. M. Jones, *Data for Biochemical Research*, Clarendon Press, Oxford, UK, 3rd edn., 1986, pp. 423–425.
29 S. Fredriksson, in *Electrofocusing and Isotachophoresis*, ed. B. J. Radola and D. Graesslin, Walter de Gruyter & Co., Berlin, Germany, 1977, pp. 71–83.
30 P. G. Righetti, G. Tudor and K. Ek, *J. Chromatogr*. 1981, **220**, 115.

Paper 8/07951J